

Motion of Droplets with Air Impinging Power Equipment for Investigation of Collision Efficiency in Icing Modeling

M. Milanez and M. Farzaneh

NSERC/Hydro-Quebec/UQAC Industrial Chair on Atmospheric Icing of Power, Network Equipment (CIGELE) and Canada Research Chair on Engineering of Power, Network Atmospheric Icing (INGIVRE), University of Quebec at Chicoutimi, Quebec, Canada G7H 2B1
www.cigele.ca

Abstract—Temporal and spatial determination of the amount and location of accumulating ice with its propagating leading edge requires an analysis of freezing flows impacting ice-prone surfaces, for example a cable/conductor or an airfoil of a wind turbine. For this purpose, ‘two fluid’ dilute droplet/air formulations entailing freezing atmospheric conditions are established in a Lagrangian framework for studying a drag/gravity ratio and droplet impingement distribution on the surfaces. A Local Collision/Capture Efficiency (LCE) measure is quantified from such assessments of the continuous flow. The LCE provides information on the characteristics of ice shape. Interchangeably used volumetric buoyancy and gravity, and the interfacial drag are externally imparted onto a droplet. The applied drag exerts an influence on droplet immersion in air and its inertia at the impacted surface. The droplet ‘virtual mass’ force is exempt from these low void fraction studies. Parametric studies entail the supercooled flow-structure interactions and profiling LCE. Illustrative examples involve a simulation of strong and weak interphasic connections in changing two-phase flow. For example, following two consecutive sudden changes of air motion, the initially departed droplet flow (re)joins air. The initial conditions of the latter stage are setup in the investigation of the droplet impingement distribution. Presented three-phase modeling is applicable to temporal predictions of an ice space, ice mass and an ice interface location on power network structures. This approach allows comparisons with complementary models involving validation studies and its utilization in future sensitivity analyses, e. g. leading to an improved C_D model for a droplet in the sub/super-cooled atmospheric conditions.

I. INTRODUCTION

ICING of super/subcooled surfaces of power network equipment (PNES) starts at the PNES locations of droplet impingement (intersections). Understanding dynamics of multiphase flow with droplets is a prerequisite for determination of intersections on PNES. Their position is crucial in understanding and modeling of icing processes, icing loads on the equipment and anti/de-icing measures. If the droplets are immersed in air flow, their landing positions are determined by the air. If inter phase droplet air drag is weak the positions also depend on the droplet flow. By developing a simple Lagrangian model for determining the droplet air flow with its PNES impingement characteristics leading to LCE distribution, a closer look into the onset of PNES icing is provided through illustrative cases.

A variety of physical and computational procedures of multiphase flow with droplets have been implemented, including Eulerian [1]-[2], Lagrangian [3] or Lagrangian-Eulerian [4] frameworks with average or instantaneous formulations [5] and ‘two fluid’ [6] or mixture [7] fluid models. Early fundamental studies of multiphase flow with cloud droplets and their impingement locations on surfaces are carried out in [8] and [9]. The droplet motion in air was studied by Makkonen [10], mainly through its relation to ice accretion on airfoils. He investigated LCE and volume weighted droplet LCE for wind turbine airfoils at different angles of attack of moderate to high speed wind flow. Droplets with a range of diameters 1.5–50 μm were used.

The studies of multiphase flows with droplets were conducted for in-cloud icing conditions by [1]. A range of droplet diameters and liquid water contents were used. Drag coefficients in single and multiphase flows as they relate to absolute or relative Re numbers were investigated in [11] and [12]. Farzaneh [13]-[14] investigated ice accretion on conductors mainly through the influence of an electric field on the impinging droplet flow. Jasinski [15] concluded that freezing atmospheric flow impinging an airfoil of a wind turbine under supercooled fog and cloud conditions may degrade its performance as much as 20 %.

The proposed Lagrangian model includes the determination of acceleration, velocity and trajectories of droplet flow in air, combined with the determination of the impingement locations and LCE [10]. A local and convective acceleration are combined into a simplified total time velocity derivative. Interfacial two-phase drag, gravity and buoyancy externally control droplet motion in air. Various drag coefficients are considered in the determination of the drag ([1] and [11]). The three-phase aspects of pre-icing stages that were studied resemble freezing conditions when, for example co-flowing and (re)joining droplet and air flows impinge on an airfoil of a wind turbine. Still and moving air affect the droplet flow, which is horizontally and vertically emitted into the domain with low-moderate velocity. A drag/gravity ratio controls the motion of droplets and air through droplet size (regarded as median volume diameter) and velocities of the contacted phases. The ratio therefore affects locations of the flow impingement and LCE distribution over a surface of NACA 3-

212 airfoil. Future work will incorporate complete air equations and phase pressure fields.

II. LIQUID/GAS FORMULATION FOR DROPLET FLOW

Dilute liquid flow is modeled in a ‘two fluid’ flow and point force Lagrangian framework. A general transport model consists of inertia, interfacial drag, buoyancy and gravity balance acting on an undeformable liquid (e. g. water) parcel:

$$\vec{F}_i = \vec{F}_d + \vec{F}_g + \vec{F}_b. \quad (1)$$

Inertia on a left side of Eq. (1) can be expressed by

$$F_i = M_L \frac{d\vec{v}_L}{dt}. \quad \text{A high Reynolds number form of a drag,}$$

gravity and buoyancy on the right side of (1) can be expressed

$$\text{by } \vec{F}_d = -0.5 C_D \rho_G A_L |\vec{v}_L - \vec{v}_G| (\vec{v}_L - \vec{v}_G), \quad \vec{F}_g = M_L \vec{g}$$

and $\vec{F}_b = \rho_L V_G \vec{g}$, respectively. Symbols M , v , t , ρ , A ,

V , g represent mass, velocity, time, density, a cross section

area, a volume and a gravity constant, respectively. Subscripts

L and G represent a liquid and gas state of a

component/phase. A flowing water droplet, denoted by

subscript d is assumed to be a spherically shaped supercooled

particle. Air (a) is a gas component. A relative Reynolds

number between phases in contact in each direction, Re_r , is

defined for a droplet flow phase as

$Re_r = \rho_a |\vec{v}_d - \vec{v}_a| D_d / \mu_a$, where D represents a diameter. If

they are two secondary phases (i. e. denoted by $g1$ and $g2$)

involved, e. g. instead of one secondary phase-air, their Re_r

can be evaluated from $Re_r = \rho_{g1, g2} |\vec{v}_{g2} - \vec{v}_{g1}| D_{g1, g2} / \mu_{g1, g2}$.

For example, a dynamic viscosity of a mixture is

$\mu_{g1, g2} = \beta_{g1} \mu_{g1} + \beta_{g2} \mu_{g2}$. The following ‘two fluid’ based

transport equations for a droplet dispersed in an air phase can

be written for two Cartesian directions

$$\zeta_i \frac{dv_{d,x}}{dt} = -\zeta_d |\vec{v}_d - \vec{v}_a| (v_{d,x} - v_{a,x}), \quad (2)$$

$$\zeta_i \frac{dv_{d,y}}{dt} = -\zeta_d |\vec{v}_d - \vec{v}_a| (v_{d,y} - v_{a,y}) + (\zeta_g - \zeta_b) g, \quad (3)$$

where coefficients are related to mass of a volume for a

specific phase, such as $\zeta_i = \rho_d \pi D_d^3 / 6$,

$\zeta_d = (\rho_a / 2) C_D \pi D_d^2 / 4$, $\zeta_g = \rho_d g \pi D_d^3 / 6$ and

$\zeta_b = \rho_a g \pi D_d^3 / 6$. Drag coefficient C_D can be estimated for

a range of relative Reynolds numbers, such as

$$C_D = \frac{c_1}{Re_r^2} + \frac{c_2}{Re_r} + c_3, \quad (4)$$

where coefficients are defined in Table I. More incomplete

and practical expression than (4) can be found, e. g. in [1]

$C_D = [(24 / Re_r)(1 + 0.15 Re_r^{0.687})]; \quad Re_r \leq 1000$

$= [0.44]; \quad Re_r > 1000$ (5)

Equations (2)-(3) can be solved for two systems of

equations for a droplet phase velocity and trajectory fields in

an air phase. When no drag or buoyancy is exerted on a

droplet, a velocity and trajectory solutions of (2)-(3) collapse

to (a) $v_{d,x}(t) = v_{d,x,0}(t_0)$, $v_{d,y}(t) = v_{d,y,0}(t_0) - g(t - t_0)$ and (b)

$$x_d(t) = x_{d,0}(t_0) + v_{d,x,0}(t - t_0), \quad y_d(t) = y_{d,0}(t_0) - (g/2)(t - t_0)^2.$$

In this study, air flow is not influenced by the phases in contact. Flows are assumed to be abruptly stopped by an airfoil of a wind turbine.

TABLE I
DRAG COEFFICIENTS [11]

c_1	c_2	c_3	Range
0.0000	18.0000	0.0000	$0.0 < Re_r < 0.1$
0.0903	22.7300	3.6900	$0.1 < Re_r < 1.0$
-3.8889	29.1667	1.2220	$1.0 < Re_r < 10.0$
-116.6700	46.5000	0.6167	$10.0 < Re_r < 100.0$
-2778.0000	98.3300	0.3644	$100.0 < Re_r < 1000.0$
-47500.0000	148.6200	0.3570	$1000.0 < Re_r < 5000.0$
578700.0000	-490.5460	0.4600	$5000.0 < Re_r < 10000.0$
5416700.0000	-1662.5000	0.5191	$Re_r > 10000.0$

Fig. 1 sketches a physical domain with the airfoil. In both cases, boundary and initial conditions for both phases are at their inlets of a Diriclet type. Boundary conditions at all other locations, such as their free sides, outlets and PNES (e. g. airfoil surfaces), are of a Neumann (natural) type. The conditions are presented in relevant subsections. A developed procedure is employed for the investigation of horizontally and vertically emitted droplet flow in air with studies of externally imparted forces for LCE characterization in airfoil applications. The multiphase study is carried out with a variety of water/droplet and air properties. The presented results include properties in freezing conditions at $T = 0^\circ C$.

III. LCE CHARACTERIZATION

The airfoil type of NACA-63212 used in this study is commonly accommodated in wind turbine blades. For practical calculation reasons, its geometrical profile is approximated by functions. The upper and lower surfaces can be approximated:

$$Y_U = -3.0425 X^6 + 10.0660 X^5 - 12.8180 X^4 \quad (6)$$

$$+ 8.0865 X^3 - 2.9254 X^2 + 0.6262 \quad (3)$$

$$Y_L = 2.3237 X^6 - 7.8878 X^5 + 10.1940 X^4 \quad (7)$$

$$- 6.4994 X^3 + 2.3589 X^2 - 0.4832 X - 0.0058$$

A ‘wetted’ (wetted) surface of the airfoil, impacted by the

droplet flow is investigated in regards to an inlet surface. The

flow impingement locations (intersections) on the airfoil are

needed for LCE calculation. The Cartesian intersections can

be determined with the following equations:

$$X_k = (-Y_{F,t+1} + Y_{O,t+1} + C_F X_{F,t+1} - C_O X_{O,t+1}) / (C_F - C_O) \quad (8)$$

$$Y_k = Y_{t+1} + C_F (X_k - X_{F,t+1}), \quad (9)$$

where

$$C_F = Y_{t+1} - Y_t / X_{t+1} - X_t, \quad (10)$$

$$C_O = Y_{O,t+1} - Y_{O,t} / X_{O,t+1} - X_{O,t}. \quad (11)$$

Symbols F , O , t and l represent flow (referred to a trajectory),

object (referred to a cylinder or an airfoil), time and location

on the object, respectively. The instant of flow impingement

on the object can be calculated as

$$(Y_k - Y_{F,t})(Y_k - Y_{F,t+1}) < 0, \quad (12)$$

$$(Y_k - Y_{O,t})(Y_k - Y_{O,t+1}) < 0. \quad (13)$$

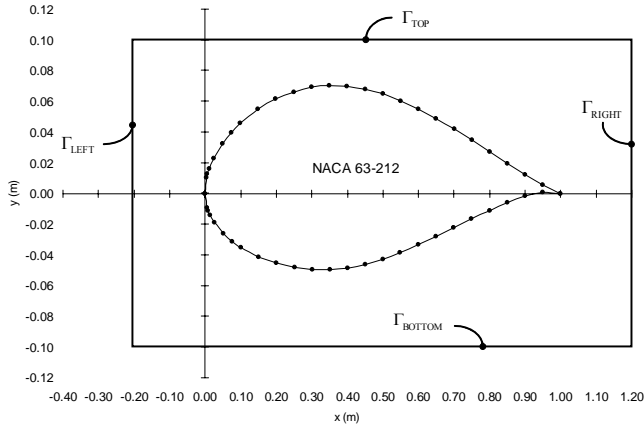


Fig. 1. Physical model with the airfoil.

Local Collision Efficiency can be defined from [10] as

$$LCE = \frac{dY_{IN}}{dL_{OUT}}, \quad (14)$$

where the surface areas (in 2D: lengths) dY_{IN} and dL_{OUT} are the distances between two locations of two adjacent trajectories: at the inlet of the computational domain and at the impact section of the airfoil (outlet), respectively. LCE in (14) can be discretized as follows

$$LCE_j = \frac{Y_{IN, F, j} - Y_{IN, F, j-1}}{L_{OUT, F-O, j} - L_{OUT, F-O, j-1}}, \quad (15)$$

where symbol j stands for j^{th} trajectory, which impacts the object (the positions at the inlet and intersection). A total approximate value of LCE can be calculated from

$$LCE = \sum_j \frac{\Delta Y_{OUT, j}}{\Delta L_{IN, j}}. \quad (16)$$

IV. DROPLET FLOW AND LCE ANALYSES

A. No-Drag and Drag Based Trajectory Comparisons

The droplet flow is horizontally emitted into a computational domain at inlet boundary Γ_{LEFT} (Fig. 1). The velocity of emitted droplet flow is $[v_{d, x, 0}, v_{d, y, 0}] = [5.0, 0.0]$ m/s, whereas the air flow velocity is $[v_{a, x}, v_{a, y}] = [0.0, 0.0]$ m/s. An initial position for the droplet flow is $[x_{d, 0}, y_{d, 0}] = [-0.2, -0.1]$ m. Some simulation parameters at $T = 0^\circ\text{C}$ are presented in Table II for inlet drag estimation. Larger relative Re and C_D exist at $T = 0^\circ\text{C}$ (lower temperature) than at $T = 20^\circ\text{C}$ (higher temperature).

TABLE II
ESTIMATED Re_r AND C_D [11]

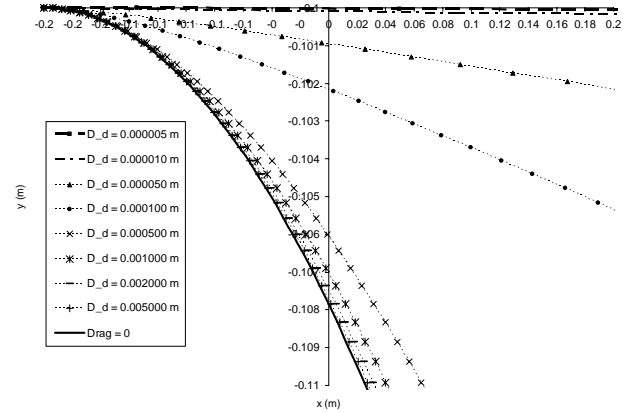
D_d (m)	$Re_{r, IN}$ (-)	C_D (-)	Range
0.000005	1.9	15.6	$1.0 < Re_r < 10.0$
0.00001	3.8	8.7	$1.0 < Re_r < 10.0$
0.00005	18.8	2.8	$10.0 < Re_r < 100.0$
0.0001	37.6	1.8	$10.0 < Re_r < 100.0$
0.0005	187.8	0.8	$100.0 < Re_r < 1000.0$
0.001	375.7	0.6	$100.0 < Re_r < 1000.0$
0.002	751.3	0.5	$100.0 < Re_r < 1000.0$

Simulated trajectories are visualized in Fig. 2. Smaller droplets with a larger drag coefficient do not depart from the initial velocity as much as larger droplets. Trajectories with a larger droplet diameter are less affected by drag resistance. It can be noted, for example that droplets with $D_d = 0.002$ m have trajectories very similar to those with excluded drag and buoyancy.

The distribution of absolute droplet velocity in still air is presented in Fig. 3. Due to the larger resistance of smaller droplets through air, both horizontal and absolute vertical droplet flow velocities are smaller than for larger droplets. Larger droplets fall under larger curvature, and at higher downward velocity than smaller droplets. Droplet flow with no drag exerted on it falls under continuously progressive absolute velocity.

B. LCE Solutions with Analysis

The Lagrangian model is used for the computation of LCE on the airfoil. The droplet diameter used in this analysis is $D_d = 0.0005$ m. Only few trajectories are graphically presented for better clarity.


 Fig. 2. Comparisons of droplet flow trajectories = $f(D_d)$.

1) Horizontally Emitted Droplet Flow

The droplet flow is emitted into the domain horizontally at inlet boundary Γ_{LEFT} with $[v_{d, x, 0}, v_{d, y, 0}] = [5.0, 0.0]$ m/s. The initial position for the droplet flow is $[x_{d, 0}, y_{d, 0}] = [-0.2, -0.1]$ m. The air flow is entering the domain at boundary Γ_{BOTTOM} . Different inlet air flow conditions entail gradually increasing velocities $[v_{a, x, 0}, v_{a, y, 0}]$, ranging from $[0.0, 0.0]$ - $[0.0, 3.0]$ m/s with increments of $[0.0, 0.05]$ m/s (Case 1-Case 7). The effect of the air flow on the droplet flow is studied with respect to the drag/gravity/(buoyancy), trajectory-airfoil intersections and LCE.

The droplets in Fig. 4 travel through still air due to initial inertia and a gravitational field, while resisted by drag and buoyancy. It should be noted that the latter is the smallest force exerted on the droplets, in an approximate range of $8.0 \cdot 10^{-10} - 9.0 \cdot 10^{-10}$ N. Increasing a speed of the upwardly directed air flow, the horizontally emitted droplet flow, which tends to move downwards, gradually gets to move upwards (at approx. $v_{a, y, 0} = 2.5$ m/s).

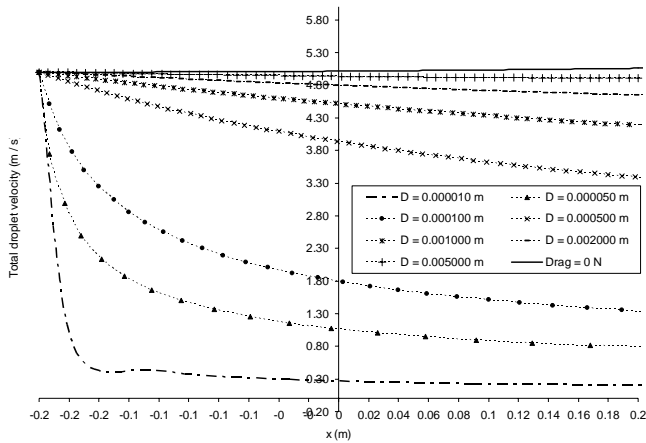


Fig. 3. Comparison of droplet flow velocities = $f(D_d)$.

Case 7 ($v_{a,y,0} = 3 \text{ m/s}$) is presented in Fig. 5, where air flow has sufficient inertia to (re)direct the droplet flow upwards. Similar situations may appear in applications involving unstable air droplet flow prior to its impact on a wind turbine. For example, let us suppose that a horizontally co-flowing carrier air with droplets separates in air and droplet flows due to sudden change in the air pressure field (e. g. depression, negative relative static pressure from the lower side of the flows). Due to their inertia (especially with larger droplets), the droplets continue to move straight, while air turns downwards. In the zone of pressure recovery, however, the air may re-turn upwards. A (re)-attachment point of the phases represent our initial conditions at the inlet boundaries of the flow.

Distribution of local LCE is shown in Figs. 6-7. The analysis is carried out based on the velocity and trajectory fields of cases 1-7 (e. g. Figs. 4-5) related to a profile of NACA 63-212 airfoil. For example, it can be noted in Fig. 4 that downward moving droplet flow impacts the airfoil, mainly on its upper surface. Fig. 5 presents a situation where droplet air flow, upwardly lifted by air, creates the same number of intersections with the airfoil on its upper and lower surfaces.

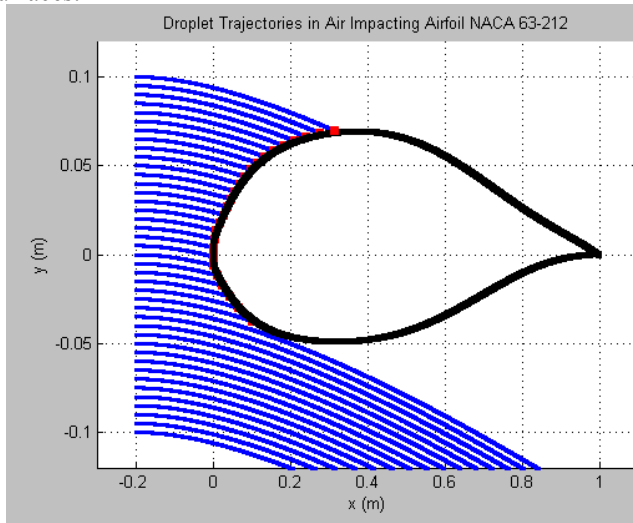


Fig. 4. The droplet flow for case 1 ($v_{a,y,0} = 0 \text{ m/s}$).

In case 5, the droplet trajectories impact the upper surface of the airfoil at more locations-interfaces than for all the other cases (see the numebr of points in Fig. 6). This situation roughly coincides with that when air flow ($v_{a,y,0} = 2 - 2.5 \text{ m/s}$) re-directs the droplet trajectories upward. LCE values decreases on the upper surface with increasing $v_{a,y,0}$. This is expected as the droplet flow impacts the airfoil's upper surface more tangentially than in cases with lower $v_{a,y,0}$. It can also be noted in Fig. 6, and confirmed in Figs. 4-5, that more trajectory-airfoil intersections are created in case 1 than in case 7.

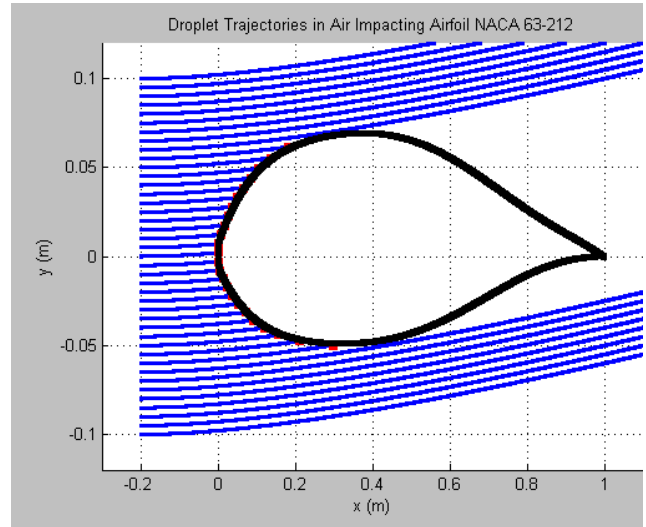


Fig. 5. The droplet flow for case 7 ($v_{a,y,0} = 3 \text{ m/s}$).

Distribution of LCE on the lower surface of the airfoil is presented in Fig. 7 and analysed in a similar manner than in Fig. 6. More intersection points and higher LCE values are observed at higer $v_{a,y,0}$. Generally, lower values of LCE are observed on the lower than on the upper surface of the airfoil, which is expected.

A total approximate LCE value is computed as a function of a drag/gravity ratio for cases 1-7 (Fig. 8).

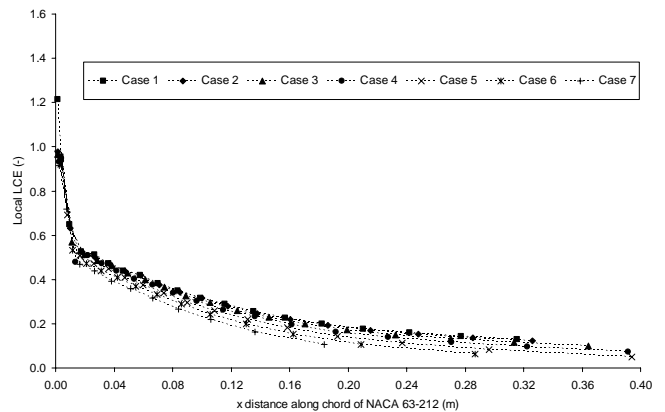


Fig. 6. LCE distribution for the upper surface of the airfoil.

The drag is evaluated based on the inlet parameters of the case. The values of a specific drag/gravity ratio are also depicted in the figure. As the drag/gravity ratio value increases, total approximate LCE decreases. This phenomena is mainly due to

the smaller surface area of droplet impact on the NACA 63-212 airfoil (wetted surface) with respect to the cases with smaller vertical air velocity. This argument can also be qualitatively estimated by comparing Figs. 4–5.

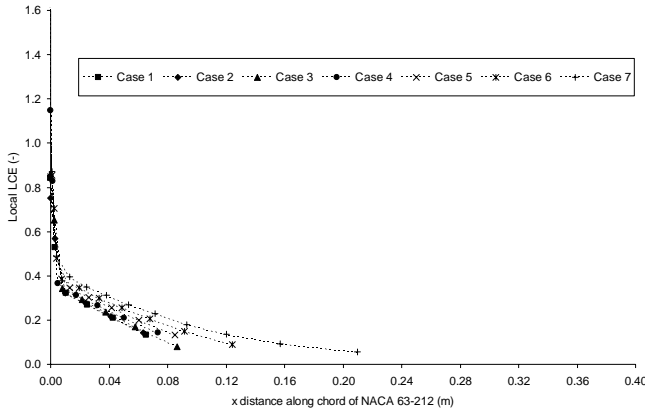


Fig. 7. LCE distribution for the lower surface of the airfoil.

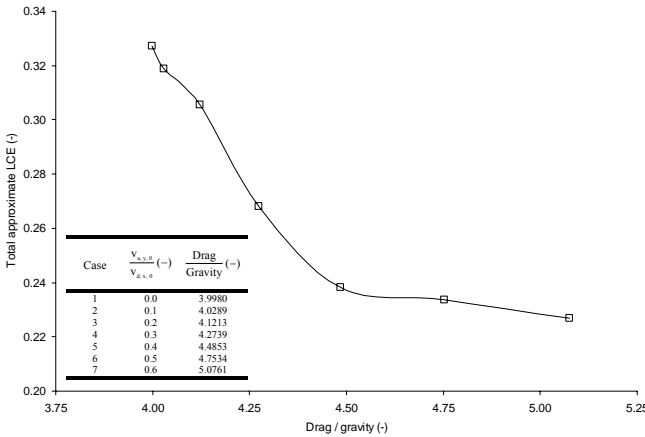


Fig. 8. Total approximate LCE on the airfoil v. s. drag/gravity.

2) Vertically Emitted Droplet Flow

Droplet flow is emitted into the domain vertically at Γ_{TOP} boundary (Fig. 1) with $[v_{d,x,0}, v_{d,y,0}] = [0.0, -2.0]$ m/s. The initial position for the droplet flow is $[x_{d,0}, y_{d,0}] = [-0.2, 0.1]$ m. Air flow is streaming from the left boundary Γ_{LEFT} of the domain with gradually increasing velocity. Similarly to section ‘1) Horizontally Emitted Droplet Flow’, in this section the effect of the air on the droplet flow is analyzed by means of the drag/gravity ratio, the location of trajectory-airfoil intersections and the distribution of LCE on NACA 63-212 airfoil. Three illustrative cases are considered and discussed.

In the first case, the droplet flow is vertically emitted in still air. Inertia and gravity drive the droplet flow, while drag and buoyancy oppose its motion. The droplet flow impinges only the upper surface of the airfoil. This can be expected from the configuration of the flow (vertical streamlines) and impacted face of the airfoil profile (e. g. see Fig. 1). Non-zero LCE values are calculated only over the upper surface of the airfoil as the flow does not impinge the lower surface. Computation confirms the observation that local values of LCE are less than

1 (see also Fig. 11).

In the second case, a vertically emitted droplet flow is pushed by rightwardly streaming air (Fig. 9). This case resembles the typical situation of flowing droplets in carrier air flow impacting a wind turbine blade. Air and droplets initially co-flows downwards towards the blade-airfoil. Due to sudden low pressure from the left, the air moves leftwards, departing from the droplets. After a subsequent change in pressure in the opposite direction, the flows merge. This instance represents the initial conditions at top Γ_{TOP} and left Γ_{LEFT} boundaries of the computational domain. The air enters the computational domain with the velocity of $[v_{a,x,0}, v_{a,y,0}] = [5.0, 0.0]$ m/s. The air flow drags the droplet flow towards the airfoil, while deflecting it to the right. Although deflected, the droplet flow does not impinge on the lower surface of the airfoil. Only LCE values for the upper surface are computed from the relevant trajectory-airfoil intersections (see also Fig. 11).

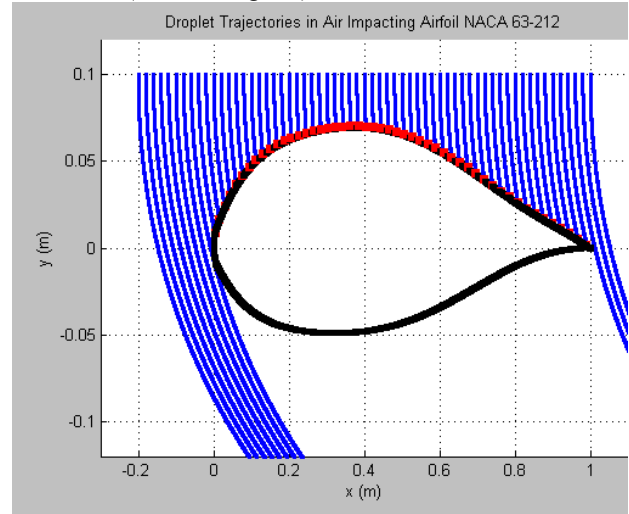


Fig. 9. The droplet flow ($v_{d,y,0} = -2$ m/s, $v_{a,x,0} = 5$ m/s).

In the third case, the air streams from the left of the domain with $[v_{a,x,0}, v_{a,y,0}] = [10.0, 0.0]$. The droplet trajectories are visualized in Fig. 10. Unlike the second case, the droplet flow is additionally deflected toward the airfoil. As the air velocity is sufficiently large, the droplet flow can reach and impact the lower surface of the airfoil at two locations. The LCE value at the second location is ~ 0.8 . This value and the LCE distribution for the upper surface of the airfoil is presented in Fig. 11. It can be observed that the LCE values for the upper surface are the largest ones, approx. along the first section of the airfoil. This is due to the larger curvature of the droplet trajectories and steep airfoil profile near its tip. On the other hand, due to the shape of the trajectories and smaller curvature of the airfoil upper surface toward its tail, the lowest LCE values are found at these locations.

The total approximate LCE values for all cases as a function of the drag/gravity ratio are listed below.

- drag/gravity = 0.96 \rightarrow LCE = 0.98 (Case 1),
- drag/gravity = 4.49 \rightarrow LCE = 0.98 (Case 2),
- drag/gravity = 12.38 \rightarrow LCE = 1.02 (Case 3).

As the ratio increases, the LCE values increase. For example, the first case shows the smaller value than the last case, mainly due to the larger wetted area on the airfoil surface (also visually compare Figs. 9-10).

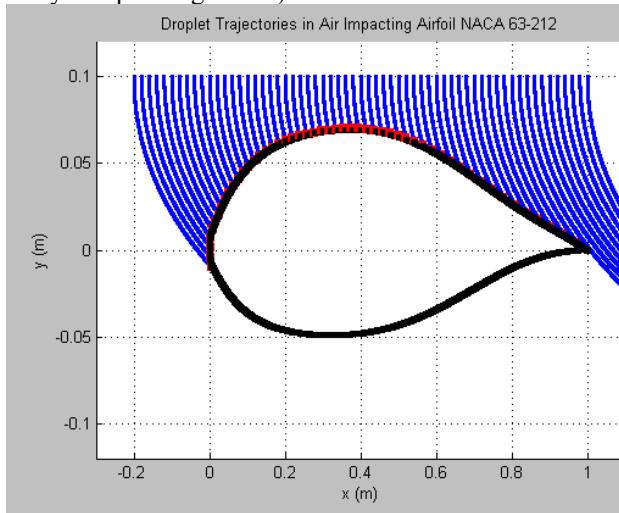


Fig. 10. The droplet flow ($v_{d,y,0} = -2$ m/s, $v_{a,x,0} = 10$ m/s).

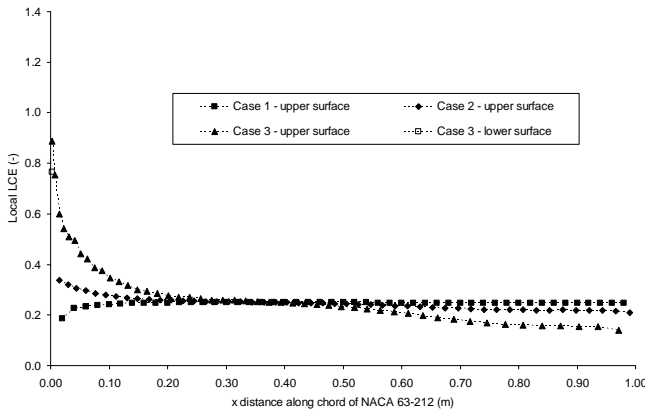


Fig. 11. LCE distribution on the airfoil for all three cases.

V. CONCLUSIONS

Droplet flow is formulated in a Lagrangian framework and a “two fluid” droplet air model. A procedure of determining a wetted surface by droplet air flow on power network equipment is established. Local and total approximate LCE values are computed from determined intersections. The study entails a variety of aspects for cases resembling the motion of sub/supercooled droplets affected by air before their impact on a wind turbine blade (e. g. with NACA 63-212 airfoil).

The droplet air flow is classified by a drag/gravity ratio. Co-flowing and rejoined droplet and air flows are analyzed. The larger the droplet diameter is, the less resistance it experiences while traveling through air. Depending on air velocity and the direction of its influence on droplet flow, the droplet impingement distribution on the airfoil surface can be significantly altered. This affects the LCE distribution and subsequent ice accretion processes on a particular surface/ice interface.

Extended applicability of the study is viewed to be in

including sophisticated flow and solid (surface) models, e. g. with rotation effects and so on, and in comparing the results with those from other models. Such comparisons provide insight into modeling of fundamental processes, such as drag of a deformable droplet in sub/supercooled conditions.

VI. ACKNOWLEDGMENT

This work was carried out within the framework of the NSERC/Hydro-Quebec/UQAC Industrial Chair on Atmospheric Icing of Power Network Equipment (CIGELE) and the Canada Research Chair on Engineering of Power Network Atmospheric Icing (INGIVRE) at Université du Québec à Chicoutimi. The authors would like to thank the CIGELE partners (Hydro-Québec, Hydro One, Électricité de France, Alcan Cable, K-Line Insulators, CQRDA and FUQAC) whose financial support made this research possible.

VII. REFERENCES

- [1] Y. Bourgault, W. G. Habashi, J. Dompierre and G. S. Baruzzi, "A finite element method study of Eulerian droplets impingements models," *Int. J. Num. Meth. In Fluids*, vol. 29, pp. 429-449, 1999.
- [2] M. Milanez, G. F. Naterer, G. Venn, G. Richardson, "Eulerian formulation for droplet tracking in dispersed phase of turbulent multiphase flow," in *2002 AIAA 32nd Fluid Dynamic Conf., AIAA Paper 2002-3182*.
- [3] J. R. Valentine, "Application of a Lagrangian Particle Tracking Scheme in a Body-Fitted Coordinate System," *Numerical Methods in Multiphase Flows*, ASME-FED 185, pp. 39-46, 1994.
- [4] J. R. Valentine, R. A. Decker, "Lagrangian-Eulerian Scheme for Flow Around an Airfoil in Rain," *International Journal of Multiphase Flow*, vol. 21, pp. 639-648, 1995.
- [5] S. Banerjee, A. M. C. Chan, "Separated Flow Models-II, Analysis of the averaged and local instantaneous formulations," *International Journal of Multiphase Flow*, vol. 6, pp. 1-24, 1980.
- [6] Y. Y. Niu, "Advection Upwinding Splitting Method to Solve a Compressible Two-Fluid Model," *International Journal for Numerical Methods in Fluids*, vol. 36, pp. 351-371, 2001.
- [7] D. D. Joseph, T. S. Lundgren, "Ensemble averaged and mixture theory equations for incompressible fluid-particle suspensions," *International Journal of Multiphase Flow*, vol. 16, pp. 35-42, 1990.
- [8] I. P. Langmuir, K. B. Blodgett, "Mathematical investigation of water droplet trajectories," *Program Press 196*, vol. 10, Report no. RL-224, 1945.
- [9] G. I. Taylor, "Notes on possible equipment and technique for experiments on icing on aircraft," British Aeronautical Research Council, R&G, no. 2024, Jan. 1940.
- [10] L. Makkonen, T. Laakso, M. Marjanjemi, K. J. Finstad, "Modelling and prevention of ice accretion on wind turbines," *Wind Engineering*, vol. 25(1), pp. 3-21, 2001.
- [11] S. A. Morsi and A. J. Alexander, "An investigation of particle trajectories in two-phase flow systems," *J. Fluid Mech.*, vol. 55 (2), pp. 193-208, Sept. 1972.
- [12] K. V. Beard and H. R. Pruppacher, "A determination of the terminal velocity and drag of small water drops by means of a wind tunnel," *J. Atmos. Sci.*, vol. 26, pp. 1066-1072, 1969.
- [13] M. Farzaneh, "Ice accretion on high voltage conductors and insulators and related phenomena," *Philosophical Transactions*, no. 358, pp. 1-35, 2000.
- [14] M. Farzaneh, "Ice accretion on energized line insulators," *International Journal of Offshore and Polar Engineering*, vol. 3, 1992.
- [15] W. J. Jasinski, S. C. Noe, M. S. Selling, M. B. Bragg, "Wind turbine performance under icing conditions," *Journal of Solar Energy Engineering*, vol. 120, pp. 60-65, 1998.